Fluorescence Dynamics of Semiconductor Nanorod Clusters Studied by Correlated Atomic Force, Transmission Electron, and Fluorescence Microscopy

Claudia Querner, Siying Wang, Ken Healy, Jessamyn A. Fairfield, Michael D. Fischbein, and Marija Drndić*

Department of Physics and Astronomy, University of Pennsylvania, Philadelphia, Pennsylvania 19104

Received: September 16, 2008; Revised Manuscript Received: October 24, 2008

Semiconductor nanocrystals have a wide range of applications as light emitters, especially in biomedical imaging. Elongated core−shell CdSe-based nanocrystals (nanorods) are particularly interesting as fluorescent markers because of their large absorption cross section, large surface area, and high brightness. While light intermittency ("blinking") in single nanorods has been studied previously, here we report the fluorescence properties of core−shell CdSe-based nanorod clusters. The time-dependent cluster fluorescence was correlated with the particle number by direct particle counting (from single nanoparticles to ∼10 000), cluster area, and the orientation and distribution of individual nanorods within these clusters. This was uniquely enabled by combined transmission electron and atomic force microscopy. In contrast to the "on/off" emission in single nanorods, we show that nanorod clusters containing as few as five nanorods exhibit a nonzero residual fluorescence in the "dark state"; that is, they can be "on" continuously, within the measurement time window of several tens of minutes. With increasing particle number, the cluster fluorescence increases in intensity and the relative fluorescence fluctuations, originating from single particle events, decrease in accordance with the central limit theorem. We report the effects of assembly patterns and nanorod orientation (on the silicon nitride substrate and relative to the laser polarization) on the fluorescence properties of the clusters. The fluorescence time-dependence of nanorod clusters at long time-scales, i.e. tens of hours, follows two characteristic trends depending on particle number and laser intensity. These data are compared to predictions made by a statistical model derived from single-particle dynamics. Finally, to investigate the possible role of charge traps on ensemble properties, we have also confirmed by electrical measurements across nanorod arrays that the electrical current exhibits statistical aging and memory effects. This complementary measurement provides a new way to relate the electrical and optical properties of nanoparticle ensembles and further suggests that filling of charge traps can possibly explain both the fluorescence and the anomalous transport dynamics of core−shell nanorod ensembles.

Introduction

Semiconductor nanocrystals have attracted wide interest for their use in biomedical imaging as fluorescence markers[1] as well as in optical devices such as light-emitting diodes[2] in flat panel displays[3] and for lasing applications,[4] owing to the highly tunable nature of their emission from the infrared to the ultraviolet regions of the spectrum.[5] In particular, CdSe-based core−shell nanorods (NRs), that is, elongated nanocrystals, have been recently identified as potentially brighter bioimaging probes than spherical particles,[6] and they have been used for live cancer cell imaging.[6,7] Other important benefits of NRs vs spherical particles for optical applications include the larger surface area that allows for the attachment of multiple linkers, the larger absorption cross section, and the faster radiative decay rates. CdSe NRs also emit linearly polarized light with a degree of polarization that depends on the aspect ratio,[8] and their emission can be switched on and off with electric fields.[9]

Light-emitting applications of NRs rely on the emission either from individual nanoparticles or from groups of several particles up to tens of thousands of them. Individual semiconductor nanocrystals, together with many other individual nanoscale emitters, have been shown to exhibit fluorescence intermittency ("blinking"),[10] an intriguing and quite universal phenomenon that still awaits a full description at the mesoscopic level. Fluorescence blinking of individual semiconductor nanocrystals exhibits a Levy power-law distribution of off-times, up to hundreds of seconds,[11] that is frequently attributed to an extra charge on the particle that quenches fluorescence via Auger processes.[10a,12] Blinking of semiconductor quantum dots is particularly important, as these systems are interesting not only for biomedical imaging but also for a large range of other applications in nanoelectronics and potential implementations of quantum computing.[13] For many applications involving single particles, such as single-photon sources and fluorescent labels, blinking is often considered to be an impediment. However, if fully understood and controlled, blinking parameters could serve as additional degrees of freedom to encode the information from the local environment, thus making nanocrystals sensitive local probes at the nanoscale. While the blinking of single semiconductor nanoparticles,[10a,11] including core and core−shell CdSe NRs,[14] has been studied, the inability to determine particle number directly has so far impeded the correlation of emission properties in groups of emitting particles with the number of particles.

Though significant progress has been made in elucidating the possible origins of single nanocrystal blinking, and in developing theoretical models to explain the blinking dynamics,[15] including

* To whom correspondence should be addressed: E-mail: drndic@physics.upenn.edu. Telephone: 215 898-5810. Fax: 215 898-2010.

10.1021/jp808252k CCC: $40.75
Published on Web 11/19/2008

trap models[10a,11b,c,12] and random walk models,[11b] less attention has been given to ensemble emission properties as well as their relation to single-particle blinking. Furthermore, the fluorescence properties of correlated particles and possible interaction effects remain to be studied. For collections of independent CdSe nanocrystals, Brokmann et al. reported that the fluorescence intensity decays as a power-law in time with an exponent between 0 and 1, as a consequence of the Levy statistics governing the blinking process of single emitters.[11e] This non-ergodic intensity decay with time was termed statistical aging. Similar aging has also been observed in the power-law time-dependence of the electrical current measured in large arrays of CdSe quantum dots, that could arise from the Levy statistics governing the electrical current in individual conducting paths.[16] Recently, however, the ergodic nature of collections of independent emitters, as manifested at long times by the steady-state ensemble emission, has been discussed by Chung et al.[17] and Tang and Marcus.[18] In order to reconcile the steady-state emission from ensembles with single-particle behavior, single-particle blinking should be showing deviations from Levy statistics at long time-scales. The probability density should decrease faster than a power-law at long off-times. Consequently, an upper bound for the single-quantum-dot power-law behavior, that is, a truncation time, $t_{off}^{max} \sim 10^3$ s, is established. However, the long measurement times required to reliably determine t_{off}^{max} make experimental confirmation difficult.

On-time probability densities deviate from the power-law at significantly shorter times ($t_{on} \sim 10$ s) than the off-time distributions and are therefore more easily experimentally accessible. This exponential truncation behavior of single-particle blinking has been most prominently displayed in recently studied CdSe NRs.[14] Here, the power-law blinking behavior is truncated at shorter time-scales ($t_{on} \sim 1-10$ s) compared to spherical nanocrystals. In addition, the truncation time for on-states decreases with increasing NR aspect ratio, which should further help to discriminate between the different blinking models that have been proposed.[15] Therefore, CdSe NRs are particularly interesting systems to study blinking in general, as well as the relationship between single-particle and ensemble behavior.

We studied the fluorescence dynamics of semiconductor NR ensembles from the single particle regime to ~10 000 particles, determined for the first time using direct particle counting, and compared the behavior of these ensembles with predictions made by a statistical model based on the dynamics of single particle fluorescence.[17] The NRs were arranged in submicron and micron-sized clusters that were either closely packed or well isolated with average spacing of tens of nanometers. We used fluorescence microscopy, atomic force microscopy (AFM), and transmission electron microscopy (TEM) to correlate the emission properties with particle number and other structural details of the emitting clusters, such as the cluster area and the orientation and distribution of individual NRs within these clusters. On short time-scales (tens of minutes), we observe in small ensembles, containing as few as 5 particles, a nonzero residual fluorescence during "dark" periods superimposed by clear blinking-like single-particle events. The fluorescence intensity from larger groups of more than ~100 NRs, and close-packed clusters with several hundreds or thousands of NRs, shows pronounced fluctuations, but with a mean intensity that is relatively constant in time for time-scales over tens of minutes. The observed fluctuations can be as high as 40% of the mean fluorescence, even in clusters containing several thousands of particles. The emission intensity scales approximately with increasing cluster size, additionally exhibiting memory effects and a dependence on irradiation intensity. Over long time-scales of hours, the fluorescence intensity is strongly time-dependent. It depends on the number of particles and laser intensity, and it can exhibit a maximum value that shifts to longer times as the number of particles increases or the laser intensity decreases, that is, it scales inversely with the number of photons absorbed per NR. To provide an additional physical insight into the microscopic origin of these phenomena, we have performed complementary current−voltage measurements across NR arrays that show a stretched-exponential time-dependence of the electrical current upon a constant voltage excitation. This observation, together with the fluorescence properties, suggests that charge trap dynamics within a disordered environment is a possible mechanism to explain the electrical and optical properties of nanoparticle clusters.

Experimental Details

We used CdSe/ZnSe/ZnS core/double shell semiconductor NRs, with the core being 5.8 ± 0.3 nm in diameter and 34 ± 3 nm in length (determined by analysis of TEM images of over 200 NRs). The CdSe core NRs were synthesized using a multiple injection method[14,19] and then subsequently capped with an intermediate ZnSe shell and an outer ZnS shell.[20] The dimensions of the core/double shell NRs are approximately 8 ± 0.7 nm × 38 ± 6 nm (determined from 50 NRs). The NRs are capped with a surfactant mixture of trioctylphosphine oxide (~1 nm), hexadecylamine (~2 nm), and dioctylamine (~1 nm) as a result of the synthesis conditions, allowing their dispersion in toluene (HPLC grade, Acros). The lengths of these capping ligands are estimates based on their extended geometry. Further details on the synthesis and characterization of the NRs can be found in the Supporting Information.

Low stress silicon nitride (Si_3N_4) membranes (Figure 1d) were used as substrates. These substrates are electron transparent in TEM and show a relatively low fluorescence background, therefore enabling correlated TEM and fluorescence measurements.[21] Gold markers, facilitating localization of the NR clusters, were patterned on the central membrane region by electron beam lithography (see Figure 1b). Substrates were always aligned such that the orientation of these markers was fixed relative to the laser polarization. This allowed the angles of the NRs relative to the laser polarization to be calculated by measuring their angles relative to the gold markers using image analysis software (ImageJ).

Solutions of NRs in toluene ($\sim 10^{-8}$ mol·L^{-1}) were deposited onto the substrate by drop-casting (~5 μL) and allowed to dry in air for ~5 min. Clusters formed readily, covering the whole substrate (cf. Figure 1), at these concentrations when keeping the solutions undisturbed for several days. Isolated NRs can be obtained by vortexing and/or centrifuging more dilute NR solutions ($\sim 10^{-9}-10^{-10}$ mol·L^{-1}) prior to their drop-casting.

Wide-field fluorescence imaging was performed at room temperature in air, using an epi-fluorescence microscope (Nikon Eclipse 80i) with a Nikon APO 100 × 0.95 NA dry objective and a 670 ± 25 nm emission filter (Chroma 670/50M). The sample was illuminated with linearly polarized light at 488 nm (100 W·cm^{-2}) with a continuous-wave solid-state laser (Coherent Sapphire). Fluorescence movies with an integration time of 0.1 s, recording 1 or 10 frame(s) per second, were captured using a thermoelectrically cooled CCD camera (Princeton Instruments Cascade 512F). The fluorescence intensity vs time of each fluorescence segment, that is, contiguous emitting area, was plotted for the duration of the entire movie. The intensity vs time of a nearby background segment, where no emitters

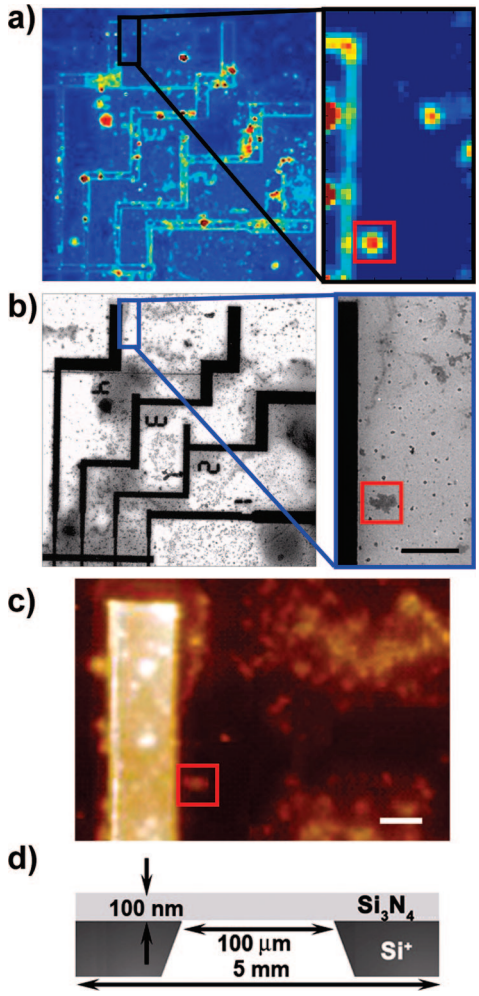

Figure 1. (a) Fluorescence micrograph (45 × 45 μm^2) of a silicon nitride (Si_3N_4) membrane with patterned gold markers and a zoom-in image (right) corresponding to the region containing the cluster from Figure 2, indicated by the red square. (b) Transmission electron micrograph (TEM) of the same region on the substrate. The scale bar in the zoom-in image, identifying the same cluster (red square), is 2 μm. (c) Atomic force micrograph (AFM) containing the same zoom-in region shown in fluorescence and TEM images in (a) and (b); the red square outlines the same cluster as in (a) and (b). The scale bar is 2 μm. (d) Schematic of the Si_3N_4 membrane used in this study: p-type silicon (Si^+) [100] wafers, covered with low stress Si_3N_4 (100 nm), were processed using photolithography, SF_6 reactive ion etching, and KOH etching to produce ~5 × 5 mm^2 square chips, each with a ~100 × 100 μm^2 region in their center where the Si_3N_4 membrane is freely suspended. Further etching (SF_6) can be carried out to reduce the membrane thickness to 30−50 nm.

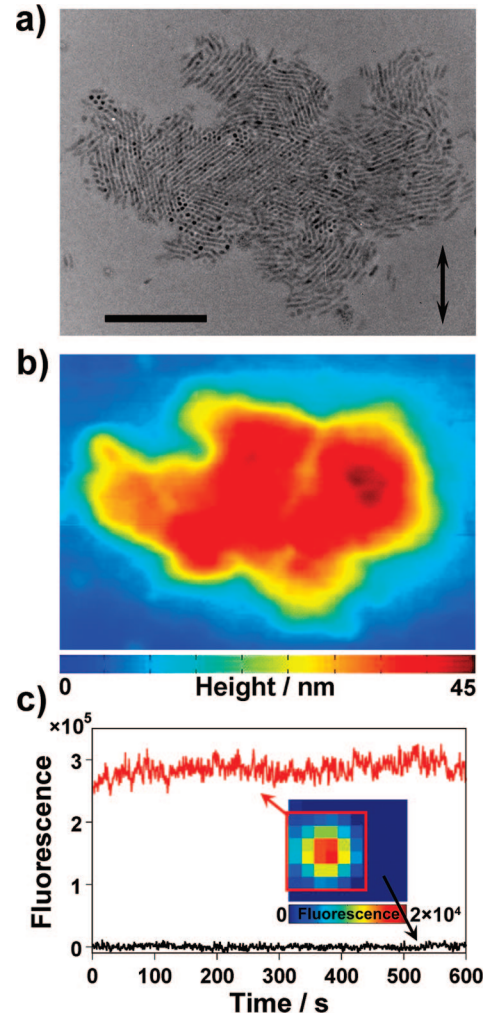

Figure 2. (a) TEM of the cluster identified in Figure 1. The arrow indicates the direction of laser polarization. The scale bar is 200 nm. (b) AFM of the same cluster. (c) Integrated fluorescence intensity vs time (red) of the region indicated by the red square in the inset, corresponding to this cluster, and a nearby background segment (black) of the same size, i.e., same number of pixels. The fluorescence movies were recorded by capturing 1 frame/s with an integration time of 0.1 s. Inset: zoom-in image of the fluorescence micrograph of this cluster.

were present, was subtracted. The mechanical drift of the microscope focal plane over time was minimized by locking the sample stage in the two opposite directions along the vertical axis, and the resulting drift over the duration of our measurements was negligible. Since we studied large nanocrystal clusters which showed at least a low level of emission continuously, it was possible to measure and compensate for any horizontal drift of the sample stage. Typical drift was 0.67 pixels/h (i.e., ~100 nm/h) and was accounted for by offsetting the position of the recorded frames appropriately during data analysis. The clusters we studied were sufficiently isolated that we were able to compute the integrated intensity over a region ~40% larger than the cluster itself, therefore eliminating any errors due to imperfect drift correction.

Following the fluorescence imaging, we carried out TEM (JEOL 2010, operating at 200 kV) and AFM (Veeco Enviro-Scope, tapping mode) of the whole membrane region and located emitting NR clusters relative to their nearest gold markers. TEM and AFM imaging was performed after the fluorescence experiment to avoid sample contamination and degradation. Figure 1 shows the correlated fluorescence (Figure 1a), TEM (Figure 1b), and AFM (Figure 1c) micrographs of the same region on a Si_3N_4 membrane (Figure 1d). To illustrate the correlation of one particular NR cluster, a red square outlining the location of this cluster is indicated in each micrograph (Figure 1a−c). We correlated over 50 emitting NR clusters using fluorescence, TEM, and AFM, and over 70 additional ones using at least one of the techniques.

For comparison, we have also measured the fluorescence of clusters containing spherical CdSe/ZnS core−shell nanocrystals (Evident Technologies) with a core diameter of 4.1 nm and an emission peak at 580 nm. The experimental setup and conditions were identical to those detailed for the NR samples, except for the emission filter (Chroma 570/60M).

Finally, to explore the effects of charging and connections to NR fluorescence, we have also performed complementary electrical transport measurements across NR arrays. Electrode

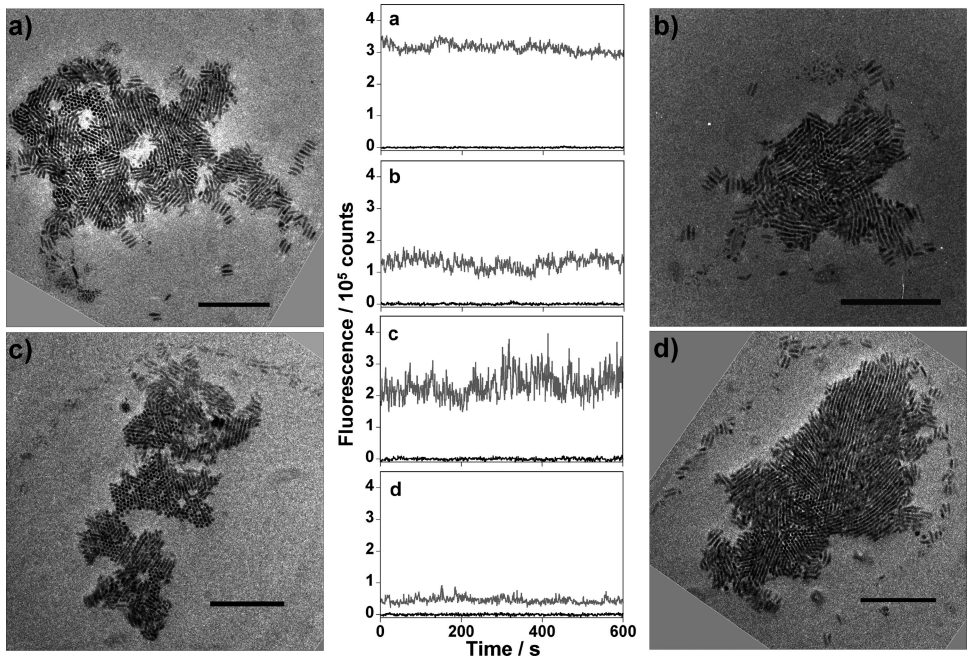

Figure 3. TEM images and corresponding integrated fluorescence vs time (gray curves; black curves are traces from adjacent background segments) of four different clusters. The fluorescence movies were recorded by capturing 1 frame/s with an integration time of 0.1 s. The "fresh" clusters, shown in (a−c), have not been exposed to light prior to the fluorescence measurement, whereas the cluster in (d) was measured after previous laser light exposure, i.e., it was "aged". Scale bars are 200 nm. The TEM images are rotated to account for the orientation of the clusters with respect to the laser polarization, which is vertically in the plane of the page (cf. arrow in Figure 2a). Fluorescence intensity vs time, TEM, and corresponding AFM images of additional clusters can be found in the Supporting Information (Figure S4).

gaps a few hundred nanometers in size were fabricated using electron beam lithography on Si_3N_4 substrates as described in ref 22, and low-noise electrical measurements were performed in vacuum,[22a,23] thus minimizing photobleaching or other degradation of the sample. Measurements were carried out in the dark, except for short periods of laser excitation (∼10 min). The NR films, deposited after device fabrication from solutions in toluene (1 μL, $c_{NR} \sim 10^{-7}$ mol·L^{-1}), covered the whole substrate.

Results

Fluorescence/TEM/AFM Correlation of NR Clusters and Direct Particle Counting. Figure 2 shows the TEM (Figure 2a), AFM (Figure 2b), and fluorescence (inset of Figure 2c) micrographs of one particular NR cluster containing ∼1500 close-packed NRs occupying a ∼0.26 μm^2 area. This cluster is also indicated by the red square in Figure 1a−c. While TEM reveals the assembly patterns and the structural details at single nm-resolution as projected in-plane, AFM provides the topographic height profile of the cluster. Both techniques are used in conjunction to determine the number of NR monolayers and to estimate the total number of particles, *N*, of the cluster. For example, we find from AFM that the maximum height of the cluster shown in Figure 2 is ∼40 nm, while from TEM it is evident that most NRs (∼93%) are oriented parallel to the substrate. Given the film thickness (40 nm) and the NR dimensions (8 × 38 nm^2), it is impossible to have standing NRs perpendicular to the substrate below the top layer of parallel NRs. Furthermore, the film thickness at different locations within a cluster is found to increase approximately in increments of the NR width (i.e., thicknesses of ∼10, 20, 30, or 40 nm are recorded), suggesting that NRs stack in monolayers parallel to the substrate. Therefore, we can conclude that the cluster is composed of up to four stacked monolayers, considering that the NR diameter is ∼8 nm and the organic shell is ∼1−2 nm. Part of these in-plane oriented NRs form columnar phases with end-to-end assembled NRs.[24] In addition, the TEM image shows that some NRs (106 out of 1500 NRs, i.e., ∼7% of the total number) form regions of vertical superlattices consisting of one layer of standing NRs, which are perpendicular to the substrate. The cluster height determined from AFM is consistent with the NR length of ∼38 nm (+ organic ligands). These assembly patterns differ from theoretical predictions based on entropically driven assembly in two dimensions.[25] Thus, the assembly and packing of NRs is not purely entropically driven, but interfacial energy and droplet drying dynamics do play a crucial role.[24,26] While we can accurately determine the absolute number of NRs in monolayers, the error in particle counting (∼5% per NR monolayer) comes from multilayer regions because only the NRs in the top layer can be accurately counted (see the Supporting Information). Even though the cluster exhibits regions of highly ordered NRs (cf. columnar phases), the overall angular distribution of the NRs is random.

The spatially integrated fluorescence intensity vs time of the cluster in Figure 2a,b is shown in Figure 2c (red curve) together with the corresponding background intensity signal (black curve). The average fluorescence intensity, measured over 600 s, is approximately constant in time, but it exhibits fluctuations around its mean intensity, I_{mean} ∼290000 counts, with a standard deviation, σ, of ∼14300 counts, or σ/I_{mean} ∼5%. These fluctuations are ∼6 times higher than the ones in the corresponding background signal, which have σ ∼2400 counts, and therefore it is clear that they originate from NR events.

Figure 3 shows four additional TEM images of close-packed NR clusters, illustrating the structural diversity of assembly patterns that can be observed, and their corresponding fluorescence intensity vs time (respectively labeled a−d). The number of particles in these and 50 additional clusters (cf. Figure S4, Table S2 in the Supporting Information) was determined by combined TEM and AFM, as described above. Table 1

TABLE 1: Structural details and fluorescence properties of NR clusters

					NR orientation[d]				
						in-plane			
cluster no.	no. of NRs[a]	area (μm^2)[b]	NR layers[c]	cluster density (NRs/μm^2)	upright (%)	±(0−30°) (%)	±(30−60°) (%)	±(60−90°) (%)	I_{mean} (counts)[e] (σ/I_{mean})
1	279	0.04	4	8305	5	76	11	9	*87 400 (48%)
2	388	0.11	4	3526	0	15	57	29	32 400 (40%) *76 000 (32%)
3	418	0.05	3	9015	2	58	8	32	72 800 (28%) *55 600 (38%)
4	449	0.11	3	4144	0	28	25	48	27 300 (12%)
5	671	0.07	4	9420	34	19	24	24	77 000 (31%) *61 500 (27%)
6 (Figure 3b)	764	0.09	3	8550	9	30	38	23	128 000 (15%)
7 (Figure 3c)	1051	0.17	3	6063	41	16	20	23	231 000 (18%) *97 000 (22%)
8	1132	0.17	3	6851	3	56	17	23	294 000 (7%)
9	1329	0.23	3	5893	38	19	20	23	180 000 (18%) *71 000 (28%)
10 (Figure 2)	1499	0.26	4	5857	7	24	34	35	288 000 (5%)
11 (Figure 3d)	1696	0.25	4	6791	7	47	26	19	*45 500 (22%)
12 (Figure 3a)	1784	0.28	4	6448	11	40	21	28	314 000 (5%)

[a] Number of particles estimated by direct counting of top layers from TEM image and extrapolation for sublayers assuming similar particle packing. [b] Cluster area determined from TEM images with ImageJ software. [c] Maximal number of NR layers constituting the cluster determined from height analysis with AFM. [d] Orientation of the NRs with respect to the substrate (upright or in-plane) and with respect to the laser polarization. [e] Mean fluorescence intensity, I_{mean}, and standard deviation, σ, indicated in percent of I_{mean}. The data preceded by an asterisk are for "aged" NR clusters.

summarizes the structural parameters of twelve selected clusters, including the five clusters shown in Figures 2 and 3. Among all the clusters studied, the percentage of standing NRs ranged between 0 and 56%. We observe that a minimum cluster size of ~250 NRs seems to be required before any standing NRs are observed. However, larger clusters (up to ~700 NRs) can be observed without a single standing NR, while even larger clusters (>700 NRs) show at least 3% of standing NRs. Possible theoretical explanations for this behavior are outside the scope of this article. Similarly, preferential orientation of NRs, and the extent of this ordering, can vary tremendously from cluster to cluster. As little as 7% or as many as 76% of the NRs were aligned within ±30° of an arbitrary reference (in this case, this reference was chosen to be the direction of the laser polarization). Neighboring NRs can be aligned to varying degrees, for example, in columnar phases or smaller regions of side-to-side oriented NRs (Figure 3a). This structural diversity of NR clusters was used to investigate the possible effects of individual parameters, such as particle number or assembly pattern, on the fluorescence properties.

Despite the large variety in structural patterns, the cluster area increases approximately linearly with the number of NRs. The slope gives a packing density of ~6000 NRs/μm^2 (Figure S5, Supporting Information). The cluster-to-cluster variation is significant, and most clusters range between 4000 and 8000 NRs/μm^2. Considering that a perfectly close-packed monolayer of planar NRs can contain 2500 NRs/μm^2, this density range is consistent with the varying thickness of the clusters up to four NR layers (cf. Table 1). For comparison, in ensembles of loose-packed NRs (cf. Figure 5 and Figure S3 in the Supporting Information), we found packing densities of ~100−500 NRs/μm^2. In some cases (cf. Figure 3c,d), the close-packed, multilayer clusters were surrounded by a "corona" of individual or loosely packed NRs, which effectively decreases the overall particle density. For consistency, we will therefore relate all emission or structural parameters to the number of NRs, rather than the cluster area, in the following discussion.

Dependence of Fluorescence Intensity on *N* and Assembly Patterns. Within a short experimental window of ~ 10 min, the fluorescence emission of the NR clusters is relatively constant in time and can therefore be represented by its mean intensity and standard deviation. Assuming that, on average, a similar fraction of NRs in each cluster are "bright", for example, about one-third of the NRs,[27] we expect a linear increase of the mean intensity with particle number. Figure 4a shows the mean fluorescence of 38 "fresh" NR clusters containing between 66 and ~1800 NRs, which have not been exposed to the laser beam prior to their measurement. It can be seen that the intensity does indeed increase with particle number. However, there is significant scatter around this trend. One factor that can contribute to the scatter is variations in the fraction of emitting NRs in each cluster. Even though we can determine the particle number in each cluster, we cannot measure directly the number of "dark" NRs. The number of "dark" NRs can be significant, since we found that about one-half of the clusters on the substrate were completely "dark", that is, they did not contain any "emitting" NRs within the experimental limit of detection. To explore other possible factors, we investigated the extent to which the assembly patterns of the clusters can be correlated to the fluorescence properties.

We find that NR orientation on the substrate relative to the laser polarization direction plays a role in determining the absolute fluorescence intensity of the clusters. In particular, it is expected that populations of NRs that are highly aligned (or perpendicular) to the laser polarization should increase (or decrease) the overall intensity. Since NRs couple to the laser field predominantly along their long axis, their emission intensity, I, depends on the angle, θ, between the NR long axis and the laser polarization, according to $I \propto \cos^2 \theta$.[8] In this context, standing NRs are perpendicular to the laser polarization and exhibit a relatively small contribution to the overall observed intensity. Similarly, simulations of radiation from dipoles in micron-scale dielectric rod-shaped particles show zero-emission from the tip.[28] Indeed, by subtracting the number of standing

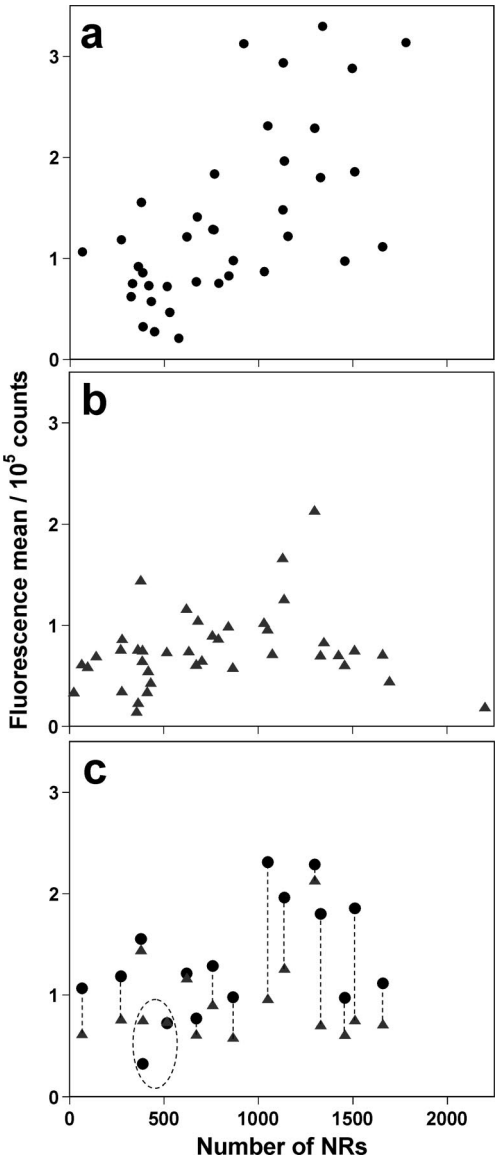

Figure 4. Mean fluorescence intensity vs number of NRs for different clusters. (a) "Fresh" NR clusters that were not (or only slightly) exposed to laser light prior to the 10 min measurement. (b) "Aged" clusters that were exposed for ~25 min to laser light prior to the corresponding measurement. (c) Comparison of 16 selected clusters that were measured "fresh" (black circles) and "aged" (gray triangles).

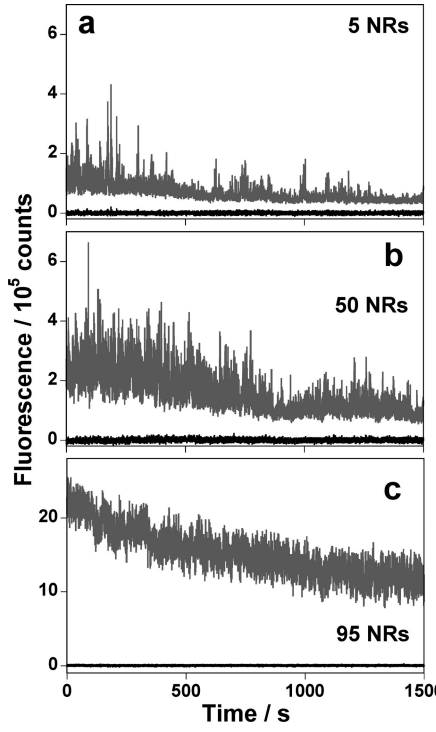

Figure 5. Fluorescence intensity vs time for loose-packed ensembles containing (a) 5 NRs, (b) 50 NRs, and (c) 95 NRs (gray curves; the black lines are the corresponding background traces). The corresponding TEMs can be found in the Supporting Information (Figure S3). Note: The corresponding fluorescence movies (integration time: 0.1 s, 10 frames/s recorded; movie length: 1500 s) were captured with a PhotonMAX camera (Princeton Instruments) instead of the Cascade 512F camera that was used throughout the rest of the study. The other experimental conditions (e.g., laser intensity) were identical.

NRs from the total number of NRs in each cluster, the linear trend from Figure 4a the becomes slightly more pronounced with improved R^2 from 0.37 (all NRs) to 0.41 (corrected NRs) (cf. Figure S6a, Supporting Information). Similarly, clusters with a higher fraction of planar NRs aligned to the laser polarization exhibit a relatively higher emission (compare, e.g., clusters #3 and #4 in Table 1).

When studying the emission from clusters that have been exposed to laser light for ~35 min prior to the fluorescence measurement,[29] that is, from the "aged" clusters, we observe an overall decrease in the mean intensity. Figure 4b shows the mean fluorescence intensity of 41 "aged" clusters. When comparing 16 specific clusters that have been measured both "fresh" and "aged" (Figure 4c), we observe that the extent of photodarkening is not the same for all of the clusters and that these variations are independent of the number of particles. The strongest decay occurred for clusters at the very center of the laser beam, that is, being exposed to the maximum laser intensity. In 2 out of 28 cases (indicated in Figure 4c), an increase in fluorescence intensity was observed. The decrease of fluorescence intensity in the majority of clusters, as well as memory effects, that is, the recovery of fluorescence after keeping the sample in the dark for some time, have been previously explained by Brokmann et al. for spherical nanocrystals in terms of statistical aging that results from power-law statistics governing single-particle blinking dynamics at short times.[11e]

Dependence of Fluorescence Fluctuations on Particle Number. In addition to studying the mean fluorescence intensity, examining fluctuations in the signal can also elucidate in more detail the underlying mesoscopic dynamics of single-particle blinking that influence the ensemble fluorescence of the clusters. Blinking from individual CdSe NRs displays similar features to those of spherical nanocrystals, with periods of "on" and "off" states.[14] One example of the time-dependent fluorescence intensity measured from a single NR on Si_3N_4 and the corresponding probability densities of on- and off-times are shown in the Supporting Information (Figure S7). In very small ensembles, containing only a few or several tens of NRs (Figure 5), we find that fluorescence fluctuations are similar to the single emitter "on/off" switching events. For example, the fluorescence vs time of a cluster containing 5 NRs (Figure 5a) shows clear blinking-like events; however, the minimum fluorescence intensity is higher than that for an adjacent background segment, for example, the ensemble is always "on" during the measurement window of 25 min. A similar continuous, but weak, fluorescence signal during "dark" periods was observed for CdSe nanowires.[30] With increasing numbers of particles, the minimum

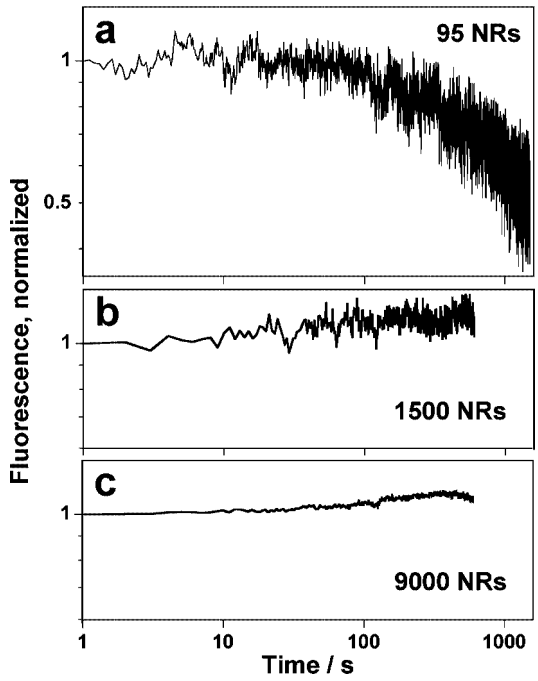

Figure 6. Fluorescence intensity vs time on a $\log_{10}-\log_{10}$ scale for NR clusters containing (a) 95 NRs, (b) ~1500 NRs, and (c) ~9000 NRs. The time resolution is 0.1 s (a) and 1 s (b,c); integration time is 0.1 s. The fluorescence intensities are normalized to give the same initial value at the beginning of the measurement.

fluorescence intensity increases, but the blinking events remain superimposed, leading to significant fluctuations. These fluctuations can be as high as 40% of the mean fluorescence, even in clusters containing several hundreds or thousands of NRs (cf. Table 1), though they tend to decrease with increasing particle number (cf. Figure S6b, Supporting Information), approximately with $\sigma/I_{mean} \propto N^{-0.5}$, which is consistent with the central limit theorem. For example, in a cluster containing ~9000 NRs, the fluctuations were 2% of the mean fluorescence intensity.

Fluorescence Dynamics Dependence on Particle Number (N < 10000). The fluorescence intensity vs time of this large cluster, containing 9000 NRs (Figure 6c), also displayed another interesting feature: its mean fluorescence intensity increased during the measurement. Specifically, it reached a maximum intensity after ~350 s, approximately 10% higher than the initial value, before decreasing by ~3% during the final 250 s of the experiment. In smaller clusters containing several hundred or thousand NRs, such a pronounced fluorescence enhancement was never observed, though slight increases could be seen occasionally (cf. Figure 3c). However, we find that, in very small ensembles, such as the one containing 95 NRs (Figure 5c), the mean fluorescence intensity decays, similar to previous reports for spherical nanocrystals.[11e] To illustrate these different behaviors depending on the particle number, Figure 6 shows the fluorescence intensity vs time curves, on a $\log_{10}-\log_{10}$ scale, for three clusters containing 95, ~1500, and ~9000 NRs, respectively. To account for the different absolute fluorescence intensities, the data have been normalized with respect to the initial intensity, that is, the intensity measured directly after beginning exposure of the samples to laser illumination. All clusters were situated in the center of the laser beam, that is, illuminated with 100 W/cm^2. These data clearly show several types of time-dependence of the fluorescence intensity (within the measurement window of 10 or 25 min, respectively): (i) an exponential decay in small ensembles (Figure 6a), (ii) an approximately constant fluorescence for "medium-sized" clusters (Figure 6b), and (iii) an increase in intensity, followed by a decrease, for large clusters (Figure 6c). These general types of fluorescence intensity time-dependence were also observed for other clusters of comparable size. Figure 6 also displays that the magnitude of relative fluctuations, σ/I_{mean}, decreases by a factor of ~3−4 for each order of magnitude increase in particle number, that is, from 20% for 95 NRs to 5% for 1500 NRs and finally to 2% for 9000 NRs, in accordance with the central limit theorem as mentioned above. This decrease of relative fluctuations implies that single NR blinking events are averaged more with an increasing particle number.

From the above discussion and the data summarized in Table 1, it can be clearly established that there is significant cluster-to-cluster variation and that measurements from a single cluster are not necessarily always consistent with the overall trend obtained from a large number of clusters, outlined above. This can be illustrated with one example of three clusters (#5, #7, and #9, cf. Table 1) with similar percentages of standing NRs and NRs approximately aligned and perpendicular to the laser polarization, but with a different total number of NRs (671, 1051, and 1329 NRs, respectively). Among these clusters, the smallest (#5) is the darkest, as expected. However, the medium cluster (#7) is the brightest (cf. Table 1). Importantly, this finding suggests that the variation in the properties of individual NRs that compose the clusters contributes significantly to ensemble properties, at least for clusters in this size range. Consequently, there are no specific patterns or NR orientation to account for *all* the observed emission behaviors. Since larger clusters seem to be needed to average out the individual NR behavior, we proceeded to study such larger clusters by depositing a 5-times more concentrated solution.

Very Large Clusters (N > 10000) and Long Time-Dependence of Fluorescence. Figure 7a shows the fluorescence intensity vs time on a $\log_{10}-\log_{10}$ scale, recorded over a total of 18.6 h, for NR clusters deposited from this more concentrated NR solution. This study at very long time-scales was used to further probe statistical aging effects. Curve NR1 corresponds to a cluster containing approximately 10000 NRs and is comparable with the results discussed above (Figure 6c). It can be seen that, after the initial period of almost constant intensity vs time, the intensity decays at long exposure times, similarly to the very small ensembles (Figure 6a); this decay occurs after ~100 s for N ~100 and after ~1000 s for N ~10 000. We then considered larger numbers of particles, that is, N ~50 000 NRs. Those were obtained by integrating the fluorescence of areas on the substrate containing several large clusters. We considered three regions of identical area (7.5 × 7.5 μm^2) and similar cluster coverage that were located in different regions of the substrate and that were consequently exposed to different laser intensities (cf. Figure 7c). Curve NR2 (black) corresponds to a cluster that was in the center of the beam, exposed to 100 W/cm^2, whereas curves NR3 (blue) and NR4 (red) correspond to clusters located toward the periphery of the beam, exposed to ~50 and ~25 W/cm^2, respectively. Compared to the smaller cluster at the same illumination intensity (curve NR1 in Figure 7a), the larger cluster (curve NR2) shows a maximum intensity that is reached after ~2000 s. The decrease of illumination intensity from 100 to 50 W/cm^2 leads to a more pronounced fluorescence intensity peak that is shifted to ~5000 s (curve NR3 in Figure 7a). For curve NR4, the cluster illuminated at the lowest intensity (25 W/cm^2), the fluorescence intensity does not reach a peak within the measurement time window (~18.6 h) but rather increases continuously. More specifically, we find that the onset of the power-law decay in ensemble fluorescence (i.e., the time of the

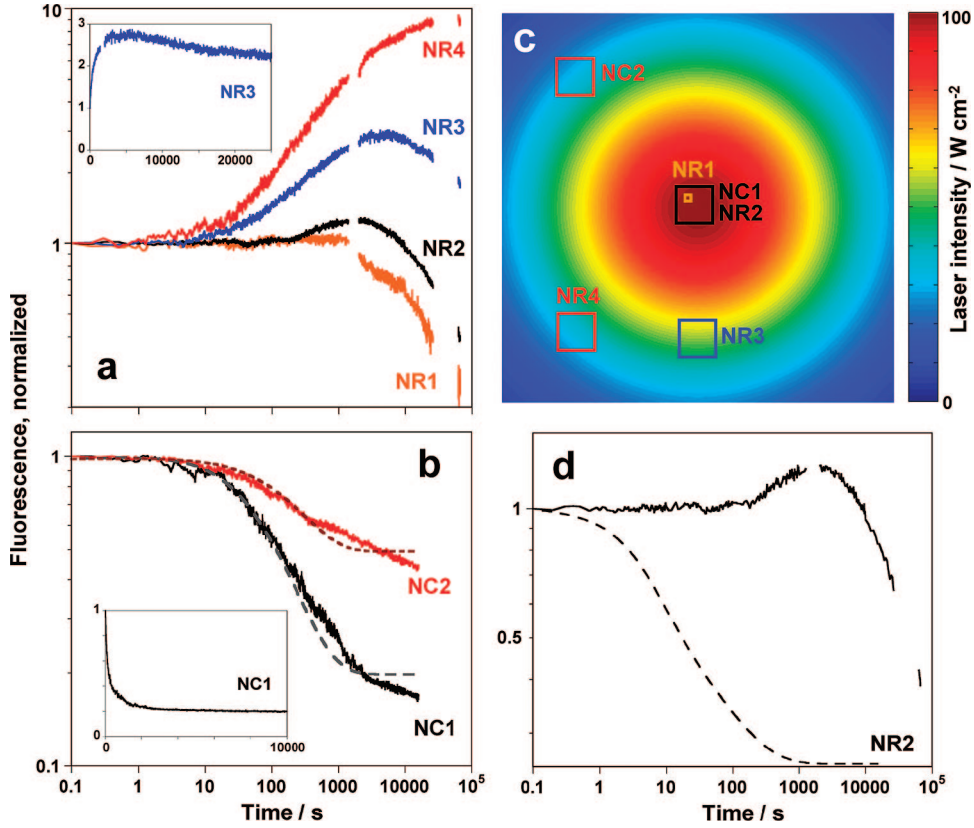

Figure 7. Fluorescence intensity vs time on a $\log_{10}-\log_{10}$ scale for (a) NR clusters containing ~10 000 NRs (NR1, orange curve) and ~50 000 NRs (NR2−NR4), as well as large clusters of (b) spherical nanocrystals (NC1, NC2) with the associated fits from the statistical model derived from single-particle blinking according to ref 17 (parameters listed in Table 2). The insets show fluorescence intensity vs time on a linear scale for NR3 and NC1. The NR samples were irradiated continuously over a period of 18.6 h, whereas the corresponding fluorescence movies were recorded during three time periods (total of ~8 h) within these 18.6 h; the missing points in the traces reflect time spans for which no data were recorded. (c) The laser beam intensity profile is well approximated by a Gaussian, with 100 W/cm^2 peak intensity. The field of view shown is ~75 × 75 μm^2; the color scale bar indicates the intensity values. The large clusters (NR2−NR4, NC1,2) were irradiated with different laser intensities, due to their differing locations relative to the center of the beam. The sizes of the indicated squares reflect the sizes of the regions studied relative to the beam profile. (d) The dashed line corresponds to the fit of the peak of trace NR2 (solid line) according to the statistical model proposed in ref 17 (parameters listed in Table 2).

TABLE 2: Fitting Parameters Used to Generate the Theoretical Intensity vs Time Curves of Nanocrystal and Nr Ensembles, Shown in Figure 7b,d

	α	μ_{on}[a]	μ_{off}[a]	t_{on}^{min} (s)	t_{off}^{min} (s)	t_{on}^{max} (s)	t_{off}^{max} (s)
NC1	0.5	0.55	0.55	10^{-5}	10^{-6}	16	1500
NC2	0.5	0.64	0.64	10^{-5}	10^{-6}	30	800
NC3	0.5	0.32	0.26	10^{-5}	10^{-6}	1.32	1500

[a] In some literature, $\mu_{on(off)}$ stand for the exponents of the on- and off-time probability density functions, $p_{nf(fn)}(t)$, that are equivalent to $1 + \mu_{on(off)}$ in this paper.

peak intensity) scales with the ratio of particle number and laser intensity, N/I_{laser}; that is, it scales inversely with the number of photons absorbed per NR.

For comparison, we have also measured the fluorescence of clusters containing spherical CdSe/ZnS core−shell nanocrystals on Si_3N_4 substrates with a similar number of particles. Figure 7b shows the fluorescence intensity vs time for two regions with large nanocrystal clusters exposed to laser intensities of 100 and 25 W/cm^2 (cf. Figure 7c). Both curves in Figure 7b show that the fluorescence intensity decreases in time, first at a slower rate (up to ~10 s) and then faster as a power-law. For the lower laser intensity, we observe that the fluorescence intensity decreases with time over the whole measurement range (curve NC2), while a higher laser intensity (curve NC1) leads to an approximately constant, apparently steady-state fluorescence, at very long times (>10 000 s).

To directly compare NC and NR intensity vs time curves, one needs to consider that the absorption cross section of spherical nanocrystals is significantly smaller than that of NRs, used in this work, by a factor of ~20.[14] To effectively have an identical absorption rate per cluster, many more spheres are necessary, compared to NRs. Qualitatively, the intensity curve of the large nanocrystal clusters could correspond to that of smaller NR clusters measured at similar intensity (e.g., NR1 and NC1, Figure 7), suggesting that, in this situation, a single NR may be treated as a small cluster of a few spherical nanocrystals. We note that a more meaningful comparison in terms of power absorbed per particle is not feasible given the intensity range available in the data set.

Anomalous Charge Transport in NRs. The fluorescence and electrical transport properties of nanoparticle ensembles should be related, since both rely on electron tunneling processes or charge diffusion, as well as on charge fluctuations in and out of the nanoparticle's core.[15,16] The characteristics of the electrical response are generally a good indicator of the underlying charge transport mechanisms at play, and both, charge transport and fluorescence, are sensitive to states on the particles' surfaces and in the environment (e.g., substrate). We therefore proceeded to measure the electrical transport on ensembles of NRs.[22c]

We have measured charge transport across monolayers and bilayers of NRs in ~200 × 600 nm^2 large electrode gaps on

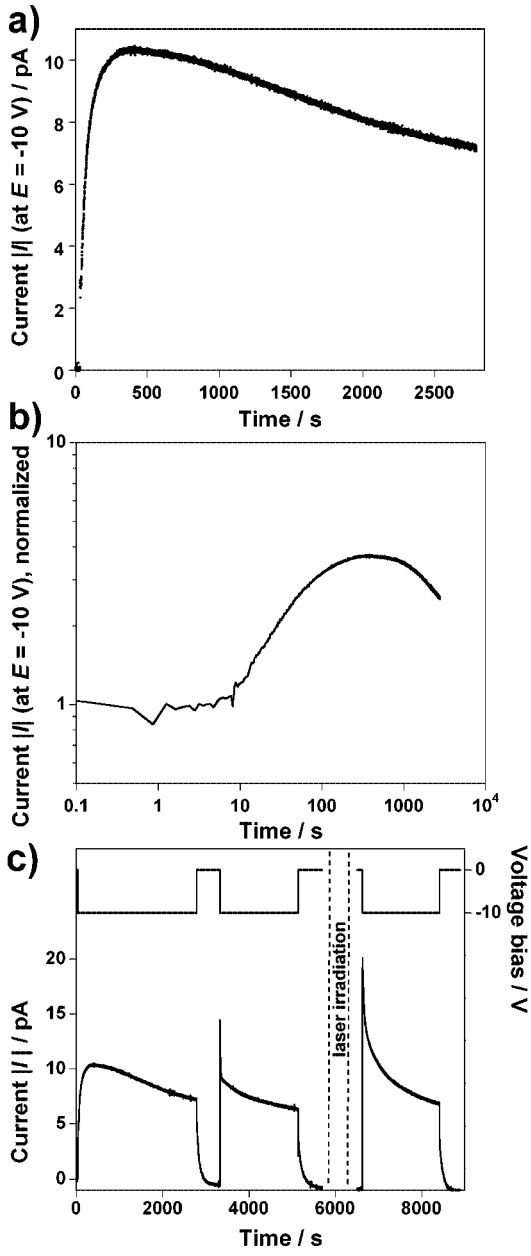

Figure 8. Absolute current vs time on a (a) linear and (b) $\log_{10}-\log_{10}$ scale at constant potential ($E = -10$ V) across a thin NR array (gap dimensions $\sim 200 \times 500$ nm^2, mono/bilayer NR coverage in the gap). The curves are qualitatively similar to the fluorescence vs time of large NR clusters, i.e., $N \geq 10\,000$, at long time-scales (Figure 7a). (c) Three consecutive measurements of the current upon application of constant voltage pulses and the effects of waiting and/or shining light onto the NR array showing the recovery or enhancement of the initial conductivity. Specifically, after the initial voltage pulse at -10 V for $\sim$50 min (also shown in (a)), the sample was kept at zero-bias for a short period of $\sim$10 min. The second voltage pulse at -10 V was then applied for $\sim$35 min, resulting in a smaller absolute current compared to that during the initial voltage pulse. During the following zero-bias phase, the sample was illuminated with green light from a laser diode for $\sim$10 min, resulting in charge extraction from the NR film and higher maximum current during the final negative voltage pulse ($\sim$35 min at -10 V).

Si_3N_4 substrates. The absolute current vs time, $|I|-t$, across one device is shown in Figure 8 for a constant voltage excitation of -10 V between Au electrodes (the background leakage current before depositing nanoparticles was <0.1 pA). The absolute current first increases in time, that is, the current gets more negative, up to $\sim$350 s, and then it decreases as a stretched-exponential function over thousands of seconds. This time-dependence resembles that observed in Figure 7a for the time-dependence of the fluorescence intensity.

Besides the nonstationary electrical response, we also observed that NR arrays exhibit electrical memory effects upon voltage excitation reminiscent of memory effects and statistical aging observed in the fluorescence upon light excitation. The electrical current through the NR film is reduced upon a second application of a voltage pulse, but it can be subsequently restored to its initial value (or to an even larger value) upon laser irradiation at zero voltage (Figure 8c).[22] Similar memory effects have been also observed in spherical NC films.[23a,31] During the voltage pulse, electrons are injected into the NR film and some of them are trapped in the film even after the voltage has been turned off. Upon illumination of the sample or by applying the opposite voltage polarity across the array, the electrons stored in charge traps can be removed from the system, thus restoring the initial current magnitude.

This nonstationary current response and memory effects in NR arrays are very similar to the time-dependent transient current response and the associated Levy processes that have been extensively studied in the context of dispersive transport in amorphous semiconductors.[32] In terms of electronic transport, the nonstationary electrical response of a system generally comes from disorder in the system, leading to a large spread of electronic states and a power-law distribution of hopping times.[32] A simple physical system consisting of electrons moving in a disordered medium between charge traps can result in a stretched-exponential time-dependence of the current for constant voltage.[32] Filling of charge traps can lead to an increase in the electrical current followed by a space-charge-limited transport and a time-decay of the current.

Discussion

Fluorescence dynamics of nanoparticle ensembles result from the cumulative blinking behavior of single particles. The most popular current theory to explain single-particle blinking assumes that neutral particles are "bright" and charged are "dark".[10a,11b,c,12] Fluctuation of charges on and around the particles can then result in fluctuations, that is, blinking in the fluorescence signal. Charge traps can originate from unpassivated surface atoms, that is, dangling surface bonds and surface transformations,[33] defects within the crystalline lattice, and surface charges.[34] Most previous studies of the role of environment[15,35] of the CdSe nanocrystal core on single-particle blinking and ensemble emission, such as the dielectric environment,[36] the substrate,[37] and the surface passivation and atmosphere,[38,39] support the charge-trapping model, where traps are assumed to be either mobile or immobile.[15] The power-law statistics of blinking is robust for a wide range of experimental conditions,[15] for example, different atmospheres, ligands, and temperatures. For particles with a thick shell, such as in this study, a similar power-law statistics of blinking occurs when particles are in air or in vacuum,[39] implying that a similar statistical (time-dependent) behavior of ensembles is expected in both atmospheres. Nanocrystals with thick shells were reported to exhibit reduced blinking.[40] Our combined experiments support the theory that fluorescence and transport properties of core−shell samples can be explained by the charge-trapping model. In the case of electrical transport, filling of charge traps can lead to the observed anomalous time-dependence of the electrical current that resembles the time-dependent fluorescence intensity (cf. Figures 7a and 8b).

Statistical Predictions of Ensemble Behavior Based on Single-Particle Dynamics. The fluorescence measurements of spherical nanocrystal ensembles performed in our work can be predicted by the particle-number and intensity-independent model by Chung et al. that provides a framework connecting single-particle blinking behavior with ensemble fluorescence.[17] We compare our data to this model and show that further development is required to quantitatively explain the intensity and particle number dependence that we have observed in ensembles.

In general, single particles emit light intermittently with probability densities of on- and off-times which follow the relationship $p_{nf(fn)}(t) = dP_{on(off)}(t)/dt$, where $1 - P_{on(off)}(t)$ are the cumulative distribution functions for on- and off-times, as expressed in eq 1,[17]

$$1 - P_{on(off)}(t) = \left(1 + t/t^{min}_{on(off)}\right)^{-\mu_{on(off)}} \exp\left(-t/t^{max}_{on(off)}\right) \quad (1)$$

where $t^{max}_{on(off)}$ are the characteristic "truncation" times of the probability densities of on- and off-times, approximately marking the truncation of the probability density from a power-law into an exponential dependence in time, $t^{min}_{on(off)}$ are the minimum durations of individual "on" and "off" blinking events, and $\mu_{on(off)}$ are the power-law exponents of the cumulative distribution functions.

The time-dependent ensemble fluorescence is described by the summation of the individual particle emission intensities vs time. It is proportional to the probability function of a collection of emitting nanocrystals, $f_{on}(t)$, which is derived from the probability densities of on- and off-times of single emitters and can be expressed analytically in its Laplace transform,[17,41]

$$f_{on}(s) = \frac{\alpha + (1-\alpha)\, p_{fn}(s)}{1 - p_{fn}(s)\, p_{nf}(s)} \frac{1 - p_{nf}(s)}{s} \quad (2)$$

where α is the fraction of nanocrystals which are initially "on" at time $t = 0$ and $p_{nf(fn)}(s)$ are the Laplace transforms of single emitters' on- and off-time probability densities, $p_{nf(fn)}(t)$. The observed fluorescence properties of ensembles therefore depend on the nature of single-particle blinking, and we further tested the applicability of this model against known parameters derived from our previous measurements of single-particle blinking.[14,15]

To compare the model to experimental ensemble intensity vs time curves, we generated $f_{on}(t)$ by setting α, $t^{min}_{on(off)}$, $t^{max}_{on(off)}$, and $\mu_{on(off)}$ to specific values, as discussed below, and by numerically calculating the inverse Laplace transform of eq 2. Simplified approximations of $f_{on}(t)$ valid over restricted time ranges, together with the known single-particle blinking parameters, were used to estimate the range of values of μ_{on}, μ_{off}, t^{max}_{on}, and t^{max}_{off} from the experimental intensity vs time curves. Specifically, for $t < t^{max}_{on}$, $f_{on}(t) = \text{const}$ when $\mu_{on} = \mu_{off}$ and it increases as $f_{on}(t) \propto 1 - At^{-(\mu_{off}-\mu_{on})}$ for $\mu_{on} < \mu_{off}$. For $t^{max}_{on} < t < t^{max}_{off}$, $f_{on}(t) \propto t^{-(1-\mu_{off})}$. These facts were used to estimate μ_{on} and μ_{off} from the slopes of the ensemble intensity vs time curves. The truncation times of the on- and off-time probabilities of single nanocrystals, t^{max}_{on} and t^{max}_{off}, were approximately determined as the times at the onset of the power-law decay and the crossover between the power-law decay and the long time steady-state, respectively. Additionally, the theoretical curves are not sensitive to the specific value of α ($\alpha = 0.5$ was used in Figure 7b), since the value of α affects $f_{on}(t)$ only at short times, outside of the time range in our measurements. Finally, $t^{min}_{on(off)}$ are the minimum durations of individual blinking events and they do not affect the theoretical curves at time-scales of our measurements. Given the number of parameters in the model, it was not feasible to determine their values via least-squares fitting, and therefore, we iterated the values of $t^{min}_{on(off)}$, $t^{max}_{on(off)}$, and $\mu_{on(off)}$ over a physically meaningful range until we generated a theoretical curve, $f_{on}(t)$, that best fits the experimental time trace over the full time range.

Figure 7b shows two theoretical curves (dashed lines) of the fluorescence intensity vs time for nanocrystal ensembles (NC1 and NC2) at two different excitation intensities. The parameters used to generate these theoretical curves are listed in Table 2. Unlike the NR ensemble emission (Figure 7a), no initial brightening was observed for spherical nanocrystals. According to the model, this implies that $\mu_{on} = \mu_{off}$, determined from the theoretical curves to be 0.55 and 0.64 for excitation intensities of 100 and 25 W/cm^2, respectively, consistent with previous single nanocrystal measurements.[15] The corresponding truncation times of on-time probabilities from the theoretical curves are $t^{max}_{on} \sim 16$ s and ~ 30 s for excitation intensities of 100 and 25 W/cm^2, respectively. These values of t^{max}_{on} and the fact that t^{max}_{on} decreases with increasing excitation intensity are also consistent with single particle measurements.[11,14] The model also yields $t^{max}_{off} \sim 1500$ and 800 s for excitation intensities of 100 and 25 W/cm^2, respectively.

To explore the possibility that decay in fluorescence at long times could be due to chemical or physical aging, we sampled the blinking probability distributions of single nanocrystals at a range of times throughout a very long measurement ($\sim$6 h). Within this time window, we studied seven single NRs and verified that the "on" and "off" probability distributions of single NRs are not time-dependent (Figure S7 in the Supporting Information): μ_{on} and μ_{off} did not vary more than 6% and 2% respectively, while t^{max}_{on} varied by 25%, which is still within the variation of t^{max}_{on} among different single NRs. No systematic trends were evident in these variations. We also note that the NRs measured consist of a double-shell structure and are less prone to bleaching than, for example, core-only nanoparticles. The time duration of several hours covers most of the data in this paper, for example, the observation of intensity peaks at $\sim$5000 s. Even without any physical aging, the ensemble fluorescence should decay in time at long times before it reaches steady-state (i.e., it should "statistically" age), so fluorescence decay does not necessarily mean that the sample is chemically or physically changing (e.g., oxidation in air or the removal of ligands under vacuum); however, we cannot completely exclude chemical and physical changes as a possible partial explanation of why some data might deviate from the statistical model.

Deviations from the Statistical Model. According to the statistical model, the maximum fluorescence intensity of ensembles should occur at a time approximately equal to t^{max}_{on}, implying that t^{max}_{on} should be $\sim$5000 s for NRs (see, e.g., curve NR2 in Figure 7a,d). However, this value is larger than that from single NR measurements ($t^{max}_{on} \sim 1$ s) and represents a clear deviation from the model. In spite of this quantitative discrepancy, we observe that the maximum of the fluorescence intensity shifts to longer times for lower laser intensity (Figure 7a, curves NR2−4), which in turn implies a longer t^{max}_{on} for lower laser intensity and is further consistent with our previous measurements of individual NRs.[14] To illustrate the expected fluorescence from the statistical model, Figure 7d also shows a calculated fluorescence intensity vs time curve (dashed line) where the values of $\mu_{on(off)}$ and t^{max}_{on} were taken from single NR measurements (see the Supporting Information), while the remaining parameters, α, $t^{min}_{on(off)}$, and t^{max}_{off} were assumed to be identical to those used to generate the theoretical curves for nanocrystals (see Table 2). While α and $t^{min}_{on(off)}$ do not influence the curve in the time range shown, the value of t^{max}_{off} influences

the slope of the fluorescence decay and the beginning of the steady-state. The onset of the fluorescence decay occurs at $t \sim t_{on}^{max} \sim 1$ s, as would be expected from single NR measurements.

To accurately describe the experimental data, the statistical model developed in ref 17 will need to be extended in the future to include the intensity and particle number dependence of the individual blinking parameters. In particular, because the onset of the power-law decay scales inversely with the number of photons absorbed per NR, as discussed above, t_{on}^{max} should scale as N/I_{laser}.

An important assumption in this model is that individual nanoparticles are treated as independent emitters.[17] This assumption may be justified, given that the probability for charges to tunnel from one NR core to the other is relatively small, since the NRs have a shell (~2 nm) and relatively long insulating ligands (~2 nm), and the tunneling probability decreases exponentially with NR−NR separation. Also, from optical and electrical transport measurements on close-packed nanoparticle arrays, it has been previously established that the interparticle coupling in these systems is very weak and that additional thermal[22b,42] or chemical[43] treatments are required to achieve stronger coupling between the particles and delocalized states across the arrays.

Conclusions

In conclusion, we studied the time-dependence and fluctuations of the fluorescence from CdSe-based core−shell NR clusters from single particles to over 10 000 particles using correlated fluorescence imaging, AFM, and TEM. In addition to allowing direct particle counting for the first time, this technique provided the ability to study the effects of nanoscale assembly patterns on the fluorescence properties (e.g., in vertical superlattices). While it has been previously shown that single NRs emit light intermittently, we report here that small ensembles of as few as 5 NRs can exhibit, in addition to single-particle-like events, a weak, nonzero fluorescence during "dark" periods, within the measurement time window. Larger clusters, containing several thousands of NRs, exhibit fluorescence approximately constant in time (over tens of minutes) that shows pronounced fluctuations which can be attributed to contributions from single-particle blinking events. For even larger clusters, these intensity fluctuations decrease relative to the mean intensity, since single particle events are averaged out following the central limit theorem.

The fluorescence intensity of NR clusters is time-dependent over long time-scales (hours), exhibiting two characteristic trends: either the intensity can decrease in time or the intensity first increases to a maximum and then decays in time according to a power-law. The nature of the time-dependence depends on the number of NRs and the laser intensity. As the particle number increases (at constant laser intensity), the time-dependence goes from an intensity decay for ensembles of up to ~100 particles to the presence of a peak in intensity for ensembles with ~1000 particles or more. As the laser intensity decreases while N remains constant, the intensity peak shifts to longer times. Thus, the onset of the power-law decay scales inversely with the number of absorbed photons per NR. We have discussed these observations in the context of a previously proposed statistical model derived from the behavior of single-particle blinking. We also carried out complementary current−voltage measurements across NR arrays showing statistical aging and memory effects, further supporting the current interpretation that traps around the particles could explain the main features of the dynamics of charge transfer processes in these systems.

The results of this study on the fluorescence properties of NR ensembles are important for any applications that consider NRs as light-emitting sources. In addition, the combined fluorescence imaging, AFM, and TEM methods, that we have introduced to allow correlation of fluorescence signals with single particle number, orientation, and distribution, will be very beneficial in future studies of nanoscale optical emitters.

Acknowledgment. This work has been supported by an Alfred P. Sloan Fellowship, NSF (NSF Career Award DMR-0449533, NSF NSEC DMR-0425780, MRSEC DMR05-20020, NSF CCF05-08346), ONR (YIP N000140410489 and N000140-510393), and a University of Pennsylvania URF grant. We thank Prof. C. H. Crouch, Prof. M. Kuno, and Dr. D. Novikov for useful discussions. We also thank Dr. I. Chung, Dr. J. Witkoskie, and Prof. J. Cao for discussing the details of the statistical model and for help with the numerical calculations of the fluorescence intensity of ensembles.

Supporting Information Available: Experimental details of the NR synthesis and their characterization, details on the direct particle counting, AFM/TEM/fluorescence correlations of additional NR clusters, tabular summary of structural parameters and emission properties of all studied clusters, fluorescence intensity vs time traces of individual NRs on Si_3N_4, and corresponding probability densities. This material is available free of charge via the Internet at http://pubs.acs.org.

References and Notes

(1) (a) Bruchez, M.; Moronne, M.; Gin, P.; Weiss, S.; Alivisatos, A. P. *Science* **1998**, *281*, 2013–2016. (b) Chan, W. C. W.; Nie, S. *Science* **1998**, *281*, 2016–2018.

(2) (a) Colvin, V. L.; Schlamp, M. C.; Alivisatos, A. P. *Nature* **1994**, *370*, 354–357. (b) Dabbousi, B. O.; Bawendi, M. G.; Onitsuka, O.; Rubner, M. F. *Appl. Phys. Lett.* **1995**, *66*, 1316–1318.

(3) (a) Coe, S.; Woo, W. K.; Bawendi, M. G.; Bulovic, V. *Nature* **2002**, *420*, 800–803. (b) Mattoussi, H.; Radzilowski, L. H.; Dabbousi, B. O.; Thomas, E. L.; Bawendi, M. G.; Rubner, M. F. *J. Appl. Phys.* **1998**, *83*, 7965–7974.

(4) Chan, Y.; Caruge, J. M.; Snee, P. T.; Bawendi, M. G. *Appl. Phys. Lett.* **2004**, *85*, 2460–2462.

(5) (a) Murray, C. B.; Norris, D. J.; Bawendi, M. G. *J. Am. Chem. Soc.* **1993**, *115*, 8706–8715. (b) Alivisatos, A. P. *Science* **1996**, *271*, 933–937. (c) Alivisatos, A. P. *J. Phys. Chem.* **1996**, *100*, 13226–13239.

(6) Fu, A.; Gu, W.; Boussert, B.; Koski, K.; Gerion, D.; Manna, L.; Le Gros, M.; Larabell, C. A.; Alivisatos, A. P. *Nano Lett.* **2007**, *7*, 179–182.

(7) (a) Yong, K. T.; Qian, J.; Roy, I.; Lee, H. H.; Bergey, E. J.; Tramposch, K. M.; He, S.; Swihart, M. T.; Maitra, A.; Prasad, P. N. *Nano Lett.* **2007**, *7*, 761–765. (b) Yong, K. T.; Roy, I.; Pudavar, H. E.; Bergey, E. J.; Tramposch, K. M.; Swihart, M. T.; Prasad, P. N. *Adv. Mater.* **2008**, *20*, 1412–1417.

(8) Hu, J. T.; Li, L. S.; Yang, W. D.; Manna, L.; Wang, L. W.; Alivisatos, A. P. *Science* **2001**, *292*, 2060–2063.

(9) Rothenberg, E.; Kazes, M.; Shaviv, E.; Banin, U. *Nano Lett.* **2005**, *5*, 1581–1586.

(10) (a) Nirmal, M.; Dabbousi, B. O.; Bawendi, M. G.; Macklin, J. J.; Trautman, J. K.; Harris, T. D.; Brus, L. E. *Nature* **1996**, *383*, 802–804. (b) Vanden Bout, D. A.; Yip, W. T.; Hu, D. H.; Fu, D. K.; Swager, T. M.; Barbara, P. F. *Science* **1997**, *277*, 1074–1077. (c) Yip, W. T.; Hu, D. H.; Yu, J.; Vanden Bout, D. A.; Barbara, P. F. *J. Phys. Chem. A* **1998**, *102*, 7564–7575. (d) Dickson, R. M.; Cubitt, A. B.; Tsien, R. Y.; Moerner, W. E. *Nature* **1997**, *388*, 355–358.

(11) (a) Kuno, M.; Fromm, D. P.; Hamann, H. F.; Gallagher, A.; Nesbitt, D. J. *J. Chem. Phys.* **2000**, *112*, 3117–3120. (b) Shimizu, K. T.; Neuhauser, R. G.; Leatherdale, C. A.; Empedocles, S. A.; Woo, W. K.; Bawendi, M. G. *Phys. Rev. B* **2001**, *63*, 205316. (c) Kuno, M.; Fromm, D. P.; Hamann, H. F.; Gallagher, A.; Nesbitt, D. J. *J. Chem. Phys.* **2001**, *115*, 1028–1040. (d) van Sark, W. G. J. H. M.; Frederix, P. L. T. M.; Bol, A. A.; Gerritsen, H. C.; Meijerink, A. *ChemPhysChem* **2002**, *3*, 871–879. (e) Brokmann, X.; Hermier, J. P.; Messin, G.; Desbiolles, P.; Bouchaud, J. P.; Dahan, M. *Phys. Rev. Lett.* **2003**, *90*, 120601.

(12) Efros, A. L.; Rosen, M. *Phys. Rev. Lett.* **1997**, *78*, 1110–1113.

(13) (a) Loss, D.; DiVincenzo, D. P. *Phys. Rev. A* **1998**, *57*, 120–126. (b) Ouyang, M.; Awschalom, D. D. *Science* **2003**, *301*, 1074–1078.

(14) Wang, S.; Querner, C.; Emmons, T.; Drndic, M.; Crouch, C. H. *J. Phys. Chem. B* **2006**, *110*, 23221–23227.

(15) For a recent review, see Cichos, F.; von Borczyskowski, C.; Orrit, M. *Curr. Opin. Colloid Interface Sci.* **2007**, *12*, 272–284, and references therein.

(16) Novikov, D. S.; Drndic, M.; Levitov, L. S.; Kastner, M. A.; Jarosz, M. V.; Bawendi, M. G. *Phys. Rev. B* **2005**, *72*, 075309.

(17) (a) Chung, I.; Bawendi, M. G. *Phys. Rev. B* **2004**, *70*, 165304. (b) Chung, I.; Witkoskie, J. B.; Cao, J. S.; Bawendi, M. G. *Phys. Rev. E* **2006**, *73*, 011106. (c) Chung, I.; Witkoskie, J. B.; Zimmer, J. P.; Cao, J.; Bawendi, M. G. *Phys. Rev. B* **2007**, *75*, 045311.

(18) (a) Tang, J.; Marcus, R. A. *J. Chem. Phys.* **2005**, *123*, 204511. (b) Tang, J.; Marcus, R. A. *J. Chem. Phys.* **2006**, *125*, 044703.

(19) Shieh, F.; Saunders, A. E.; Korgel, B. A. *J. Phys. Chem. B* **2005**, *109*, 8538–8542.

(20) Reiss, P.; Carayon, S.; Bleuse, J.; Pron, A. *Synth. Met.* **2003**, *139*, 649–652.

(21) (a) Koberling, F.; Mews, A.; Philipp, G.; Kolb, U.; Potapova, I.; Burghard, M.; Basche, T. *Appl. Phys. Lett.* **2002**, *81*, 1116–1118. (b) Koberling, F.; Kolb, U.; Philipp, G.; Potapova, I.; Basche, T.; Mews, A. *J. Phys. Chem. B* **2003**, *107*, 7463–7471.

(22) (a) Fischbein, M. D.; Drndic, M. *Appl. Phys. Lett.* **2006**, *88*, 063116. (b) Hu, Z.; Fischbein, M. D.; Drndic, M. *Nano Lett.* **2005**, *5*, 1463–1468. (c) Querner, C.; Fischbein, M. D.; Drndic, M. Unpublished results.

(23) (a) Fischbein, M. D.; Drndic, M. *Appl. Phys. Lett.* **2005**, *86*, 193106. (b) Fischbein, M. D.; Drndic, M. *Nano Lett.* **2007**, *7*, 1329–1337.

(24) He, J.; Zhang, Q.; Gupta, S.; Emrick, T.; Russell, T. P.; Thiyagarajan, P. *Small* **2007**, *3*, 1214–1217.

(25) Bates, M. A.; Frenkel, D. *J. Chem. Phys.* **2000**, *112*, 10034–10041.

(26) Querner, C.; Fischbein, M. D.; Heiney, P. A.; Drndic, M. *Adv. Mater.* **2008**, *20*, 2308–2314.

(27) Ebenstein, Y.; Mokari, T.; Banin, U. *Appl. Phys. Lett.* **2002**, *80*, 4033–4035.

(28) Li, C.; Kattawar, G. W.; You, Y.; Zhai, P.; Ying, P. *J. Quant. Spectrosc. Radiat. Transfer* **2007**, *106*, 257–261.

(29) The laser light was blocked from the sample for less than 1 min between initial exposure/first fluorescence measurement and the subsequent fluorescence measurement.

(30) (a) Protasenko, V. V.; Hull, K. L.; Kuno, M. *Adv. Mater.* **2005**, *17*, 2942–2949. (b) Glennon, J. J.; Tang, R.; Buhro, W. E.; Loomis, R. A. *Nano Lett.* **2007**, *7*, 3290–3295. (c) Glennon, J. J.; Buhro, W. E.; Loomis, R. A. *J. Phys. Chem. C* **2008**, *112*, 4813–4817.

(31) (a) Morgan, N. Y.; Leatherdale, C. A.; Drndic, M.; Jarosz, M. V.; Kastner, M. A.; Bawendi, M. G. *Phys. Rev. B* **2002**, *66*, 075339. (b) Ginger, D. S.; Greenham, N. C. *J. Appl. Phys.* **2000**, *87*, 1361.

(32) (a) Scher, H.; Montroll, E. W. *Phys. Rev. B* **1975**, *12*, 2455–2477, and references therein. (b) Orenstein, J.; Kastner, M. A. *Phys. Rev. Lett.* **1981**, *46*, 1421–1424. (c) Tiedje, T.; Rose, A. *Solid State Commun.* **1981**, *37*, 49–52. (d) Baranovskii, S. D.; Karpov, V. G. *Sov. Phys. Semicond.* **1985**, *19*, 336–337.

(33) Hess, B. C.; Okhrimenko, I. G.; Davis, R. C.; Stevens, B. C.; Schulzke, Q. A.; Wright, K. C.; Bass, C. D.; Evans, C. D.; Summers, S. L. *Phys. Rev. Lett.* **2001**, *86*, 3132–3135.

(34) (a) Krauss, T. D.; Brus, L. E. *Phys. Rev. Lett.* **1999**, *83*, 4840–4843. (b) Krishnan, R.; Hahn, M. A.; Yu, Z. H.; Silcox, J.; Fauchet, P. M.; Krauss, T. D. *Phys. Rev. Lett.* **2004**, *92*, 216803.

(35) Verberk, R.; Chon, J. W. M.; Gu, M.; Orrit, M. *Phys. E* **2005**, *26*, 19–23.

(36) Issac, A.; von Borczyskowski, C.; Cichos, F. *Phys. Rev. B* **2005**, *71*, 161302.

(37) (a) Uematsu, T.; Maenosono, S.; Yamaguchi, Y. *J. Phys. Chem. B* **2005**, *109*, 8613–8618. (b) Kimura, J.; Uematsu, T.; Maenosono, S.; Yamaguchi, Y. *J. Phys. Chem. B* **2004**, *108*, 13258–13264.

(38) Koberling, F.; Mews, A.; Basche, T. *Adv. Mater.* **2001**, *13*, 672–676.

(39) Muller, J.; Lupton, J. M.; Rogach, A. L.; Feldmann, J.; Talapin, D. V.; Weller, H. *Appl. Phys. Lett.* **2004**, *85*, 381–383.

(40) (a) Chen, Y.; Vela, J.; Htoon, H.; Casson, J. L.; Werder, D. J.; Bussian, D. A.; Klimov, V. I.; Hollingsworth, J. A. *J. Am. Chem. Soc.* **2008**, *130*, 5026–5027. (b) Mahler, B.; Spinicelli, P.; Buil, S.; Hermier, J. P.; Dubertret, B. *Nat. Mater.* **2008**, *7*, 659–664.

(41) Bardou, F.; Bouchard, J. P.; Aspect, A.; Cohen-Tannoudji, C. *Lévy Statistics and Laser Cooling: How Rare Events Bring Atoms to Rest*; Cambridge University Press: Cambridge, U.K., 2002.

(42) Drndic, M.; Jarosz, M. V.; Morgan, N. Y.; Kastner, M. A.; Bawendi, M. G. *J. Appl. Phys.* **2002**, *92*, 7498–7503.

(43) (a) Yu, D.; Wang, C. J.; Guyot-Sionnest, P. *Science* **2003**, *300*, 1277–1280. (b) Jarosz, M. V.; Porter, V. J.; Fischer, B. R.; Kastner, M. A.; Bawendi, M. G. *Phys. Rev. B* **2004**, *70*, 195327. (c) Talapin, D. V.; Murray, C. B. *Science* **2005**, *310*, 86–89. (d) Porter, V. J.; Geyer, S.; Halpert, J. E.; Kastner, M. A.; Bawendi, M. G. *J. Phys. Chem. C* **2008**, *112*, 2308–2316.

JP808252K